RESEARCH ARTICLE

Hierarchical control of differential steering for four-in-wheel-motor electric vehicle

Jie Tian[ORCID]*, Mingfei Yang

College of Automobile and Traffic Engineering, Nanjing Forestry University, Nanjing, China

* njtianjie@163.com

Abstract

The purpose of this paper is to study the control of differential steering for four-in-wheel-motor electric vehicles. The so-called differential steering means that the front wheel steering is realized through the differential driving torque between the left and right front wheels. With the consideration of tire friction circle, a hierarchical control method is proposed to realize the differential steering and the constant longitudinal speed simultaneously. Firstly, the dynamic models of the front wheel differential steering vehicle, the front wheel differential steering system and the reference vehicle are established. Secondly, the hierarchical controller is designed. The upper controller is to obtain the resultant forces and resultant torque required by the front wheel differential steering vehicle tracking the reference model through the sliding mode controller. In the middle controller, the minimum tire load ratio is selected as the objective function. Combined with the constraints, the resultant forces and resultant torque are decomposed into the longitudinal and lateral forces of four wheels by the quadratic programming method. The lower controller provides the required longitudinal forces and tire sideslip angles for the front wheel differential steering vehicle model through the tire inverse model and the longitudinal force superposition scheme. Simulation results show that the hierarchical controller can guarantee the vehicle to track the reference model well on both of the high and low adhesion coefficient road with all of the tire load ratios smaller than 1. It can be drawn that the control strategy proposed in this paper is effective.

Introduction

Electric vehicles driven by hub motors have become one of the research hotspots because of their advantages of energy saving, environmental protection, simple structure and easy to realize the integrated control [1, 2]. For these multi-actuated electric vehicles, a lot of research have been done, such as the fault-tolerant control [3], the chassis coordinated control [4, 5], the integrated vehicle-following control [6–8], the energy management strategy [9–11], the battery state-of-charge (SOC) estimation [12–14], the driving modes [15–17], the strength analysis of key components [18, 19] and so on. In addition, their appearances also make the differential steering possible, which can be used not only to assist the driver to turn the vehicle [20–23], but also as a backup system [24–28] and even the only steering system of the vehicle

[2, 29, 30], which can further simplify the structure of the vehicle. Among them, the literatures [2, 25–30] are most related to this study.

To realize the yaw control by the differential steering, an integral sliding mode control (ISMC) was proposed for in-wheel-motor (IWMD) electric vehicles. In order to eliminate the chattering effect, an adaptive super-twisting control approach was proposed to deal with the disturbances with unknown boundaries. The simulation results verified the effectiveness of the proposed controller [25]. The dynamic model differential steering vehicle (DSV) was established. The sliding mode controller was designed for the DSV to track the yaw rate and sideslip angle of the traditional front-wheel steering vehicle with neutral steering characteristics. By comparing with the designed controller for the skidding steering vehicle (SSV), the simulation results proved the possibility of the differential steering in case of steering failure [26]. In order to realize the four-wheel differential steering function of an in-wheel motor (IWM) driven electric vehicle (EV), the decoupling and fractional PID controllers were designed for the four-wheel steering vehicle (4WSV) to obtain the front and rear wheel steering angles. Then the sliding mode controller (SMC) and torque distributor were designed to control the four-wheel differential steering vehicle (4WDSV) to have the same yaw rate as the 4WSV. And the simulation results verified the effectiveness of the proposed controllers [27].

The H_∞ observer-based schema was employed for IM EVs differential steering control with rollover consideration to achieve the yaw rate tracking by differential steering and minimize the rollover risk. And the simulation results proved the effectiveness of the proposed controller [28]. A differential steering fully realized by the drive torque differences was presented. A planar and non-linear vehicle model was built, a full state feedback control system based on linear quadratic regulator (LQR) principle was developed for higher speeds to track the reference sideslip angle and yaw rate, and a simple PI angle tracking controller were proposed for lower speeds to track the reference steering input. Various simulation experiments demonstrated that the differential steering system (DSS) can be a useful alternative to conventional steering [29].

Using the robust H_∞ controller to control the forward speed and yaw rate, a differential steering by the input torque of the four wheels was achieved for an independent four-wheel drive electric vehicle (EV). By comparing with the all-wheel drive (AWD), the rear wheel drive (RWD), and the front wheel drive (FWD), the effectiveness of the robust controller was proved, which showed that the differential steering can effectively maneuver the vehicle under different driving conditions [30]. Considering the strong coupling between mechanical and control components of the differential steering vehicle, three design objectives and three constraints were defined for its dynamic, steady and low-speed steering performance, and optimization was carried out through multi-objective genetic algorithm based on iteratively updated neural network-based response surface metamodels. The results indicated that vehicles equipped with the differential steering can provide convincing steering performance [2].

To sum up, all of the above documents have realized the tracking of the reference yaw rate and even the reference centroid sideslip angle of the differential steering vehicle through the design of various controllers, and some even considered the vehicle rollover problem. In a word, the feasibility of differential steering has been confirmed to a certain extent. However, the above studies almost assumed that the vehicle speed was constant during the steering, and does not consider the nonlinearity of the tire, let alone the friction circle of the tire. That is to say, when the vehicle is driving at a constant speed and turning at the same time, the tires may not meet the two needs in the reality. In addition, if the load on the one side front wheel decreases sharply during the steering, it will also cause the wheel to be unable to generate enough driving force, which will lead to the failure of differential steering. In order to ensure

that differential steering can be used on real vehicles in the future, it is necessary to consider the friction circle of the tire to conduct in-depth research on the effectiveness of differential steering.

The contribution of this paper lies in: (1) Under the condition of considering the tire attachment circle, the front wheel differential steering is realized while ensuring the constant vehicle speed; (2) In order to track the longitudinal speed, the lateral speed and the yaw rate of the reference model, a sliding mode controller is designed to obtain the longitudinal, lateral resultant forces, and the resultant moments required by the front wheel differential steering vehicle (FWDSV); (3) Taking the minimum tire load ratio as the objective function, and the restrictions of tire attachment circle, wheel motor driving torque, resultant force and resultant moment as the constraints, the longitudinal and lateral forces required by each wheel are obtained through quadratic programming; (4) On this basis, through the tire inverse model and the superposition scheme, the longitudinal and lateral forces required by the four wheels are converted into the input parameters required by the FWDSV to complete the closed-loop control.

The rest of this paper is organized as follows the FWDSV, the front wheel differential steering system (FWDSS) and the reference model are described in Section II. In Section III the hierarchical control system including the upper, middle and low controllers is designed. Simulations and discussion are carried out in Section IV. Final conclusions are drawn in the Section V.

Dynamic models

In this section, three dynamic models are established, including the FWDSV model, the FWDSS model and the reference model. The FWDSV model is used to generate the actual longitudinal speed, lateral speed and yaw rate according to the longitudinal and lateral forces of the four wheels. The FWDSS model is used to obtain the actual longitudinal forces required by the front wheels according to the front wheel steering angle generated by the differential steering vehicle. The reference model is used to generate the desired longitudinal velocity, lateral velocity and yaw rate according to the given front wheel steering angle.

Front wheel differential steering vehicle model

The four-in-wheel-motor (4IWM) EV studied in this paper adopts the differential steering system to realize the normal front wheel steering function. In order to simplify the dynamic model, the pitch motion, roll motion and parameter uncertainty of the vehicle are ignored. The resulting vehicle plane dynamic model is shown in Fig 1.

The vehicle dynamic equation obtained from Fig 1 is as follows:

$$\begin{cases} m(\dot{v}_x - v_y\omega) = F_{xd} \\ m(\dot{v}_y + v_x\omega) = F_{yd} \, , \\ I_Z\dot{\omega} = M_d \end{cases} \tag{1}$$

$$F_{xd} = F_{xfl} + F_{xfr} + F_{xrl} + F_{xrr}, \ F_{yd} = F_{yfl} + F_{yfr} + F_{yrl} + F_{yrr}, \ M_d = l_f(F_{yfl} + F_{yfr}) - l_r(F_{yrl} + F_{yrr}) + l_s(F_{xfr-}F_{xfl}),$$

where, m is the total mass of the vehicle, v_x and v_y are the longitudinal and lateral velocities respectively, $\dot{v}_x$ and $\dot{v}_y$ are the longitudinal and lateral accelerations respectively, ω is the yaw rate, F_{xd}, F_{yd} and M_d are the longitudinal resultant force, lateral resultant force and resultant torque of the FWDSV model, F_{xij} ($i = f, r, j = l, r$) represents the longitudinal forces of four wheels, F_{yij} ($i = f, r, j = l, r$) represents the lateral forces of four wheels, I_z is the yaw moment of
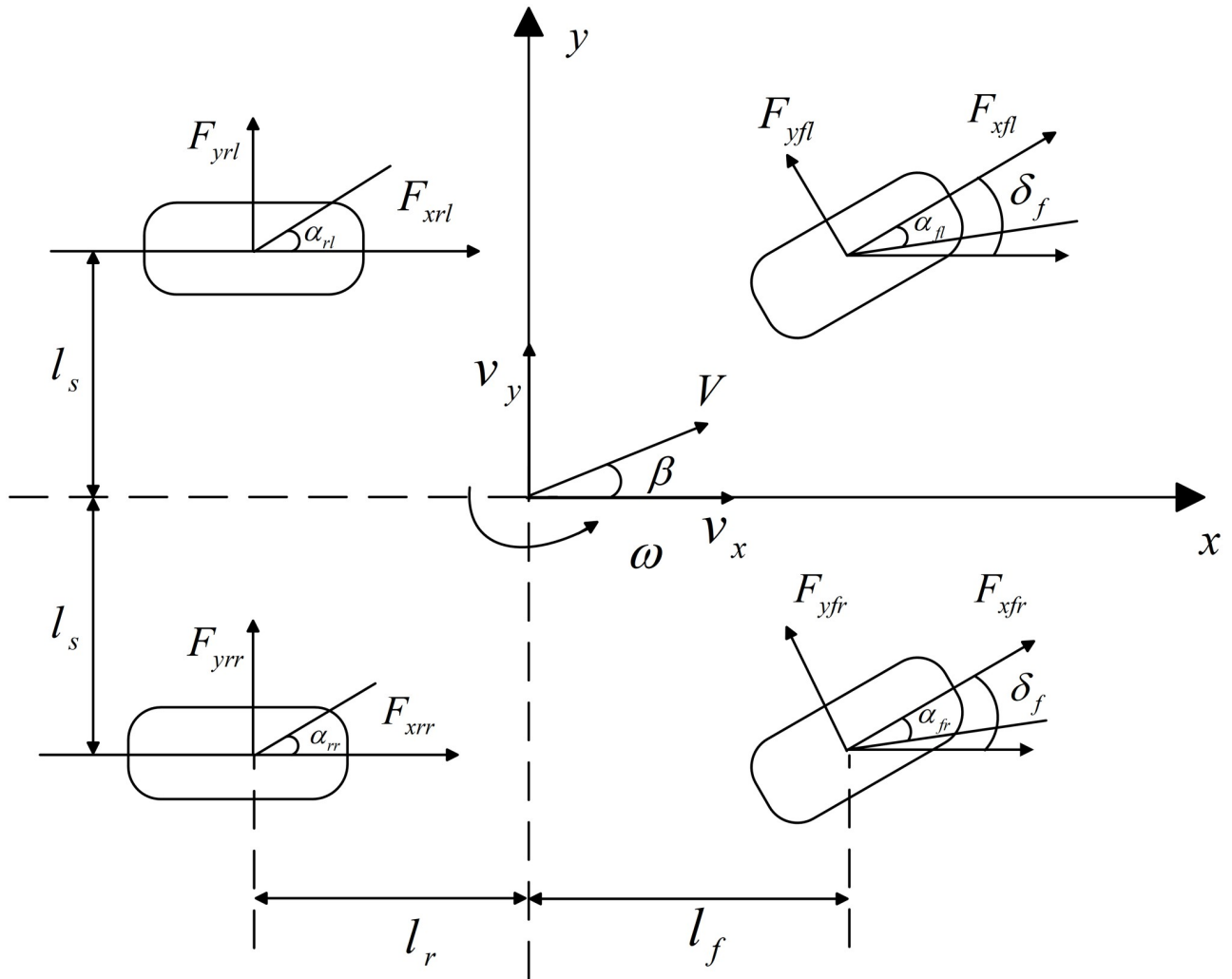
Fig 1. Vehicle plane dynamic model.

inertia, l_f and l_r are respectively the distances between the vehicle centroid and the front and rear axles, l_s is half of the wheel-track.

Remark 1. F_{xd}, F_{yd} and M_d of Eq (1) can be obtained by the upper controller, which makes the FWDSV model track the longitudinal velocity, the lateral velocity and the yaw rate of the reference model.

Considering that the wheel steering angle is small and only the front wheels turn, then

$$F_{yij} = k_i a_{ij} (i = f, r, j = l, r),\qquad(2)$$

$$\begin{cases} \alpha_f = \alpha_{fl} = \alpha_{fr} = -\beta - \dfrac{l_f \omega}{v_x} + \delta_f \\[2mm] \alpha_r = \alpha_{rl} = \alpha_{rr} = -\beta + \dfrac{l_r \omega}{v_x} \end{cases},\qquad(3)$$

where, $k_i(i = f, r)$ is the front/rear wheel cornering stiffness, $\alpha_{ij}(i = f, r, j = l, r)$ is the tire sideslip

angle of front/rear left/right wheel, $a_i (i = f, r)$ is the front/rear tire sideslip angle, β is the sideslip angle, δ_f is the front wheel steering angle.

Substituting Eqs (2) and (3) into Eq (1), then Eq (1) can be rewritten as:

$$\begin{cases} m(\dot{v}_x - v_y \omega) = F_{xfl} + F_{xfr} + F_{xrl} + F_{xrr} \\ m(\dot{v}_y + v_x \omega) = k_f \alpha_{fl} + k_f \alpha_{fr} + k_r \alpha_{rl} + k_r \alpha_{rr} \\ I_Z \dot{\omega} = l_f k_f (\alpha_{fl} + \alpha_{fr}) - l_r k_r (\alpha_{rl} + \alpha_{rr}) + l_s (F_{xfr} - F_{xfl}) \end{cases} . \tag{4}$$

Remark 2. When $F_{xij} (i = f, r, j = l, r)$ and $\alpha_{ij}(i = f, r, j = l, r)$ are obtained, v_x, v_y and ω of the FWDSV model can be obtained. Therefore, it is necessary for the middle controller to decompose F_{xd}, F_{yd} and M_d into $F_{xij} (i = f, r, j = l, r)$ and $F_{yij} (i = f, r, j = l, r)$ of each wheel, and then further convert $F_{yij} (i = f, r, j = l, r)$ into the sideslip angles of each wheel and the longitudinal forces of the front wheels by the lower controller.

And the corresponding vertical load of each wheel can be expressed as:

$$\begin{cases} F_{zfl} = \dfrac{m}{l_f + l_r} \left(\dfrac{l_r g}{2} - \dfrac{a_x h}{2} - \dfrac{a_y h l_r}{2 l_s} \right) \\[2ex] F_{zfr} = \dfrac{m}{l_f + l_r} \left(\dfrac{l_r g}{2} - \dfrac{a_x h}{2} + \dfrac{a_y h l_r}{2 l_s} \right) \\[2ex] F_{zrl} = \dfrac{m}{l_f + l_r} \left(\dfrac{l_f g}{2} + \dfrac{a_x h}{2} - \dfrac{a_y h l_f}{2 l_s} \right) \\[2ex] F_{zrr} = \dfrac{m}{l_f + l_r} \left(\dfrac{l_f g}{2} + \dfrac{a_x h}{2} + \dfrac{a_y h l_f}{2 l_s} \right) \end{cases} , \tag{5}$$

where, h is the height from the vehicle centroid to the ground, g is the gravitational acceleration.

Front wheel differential steering system model

Fig 2 shows the structure of front wheel differential steering system, where T_{fl} and T_{fr} are the driving torques of the left and right front wheels.

The dynamic equation of FWDSS model established by Fig 2 is as follows:

$$\begin{cases} J_e \ddot{\delta}_f + b_e \dot{\delta}_f = \Delta M + \tau_a - \tau_f \\ \tau_\alpha = \tau_{\alpha r} + \tau_{\alpha l} = 2 k_f \alpha_f l^2 / 3 \\ \Delta M = \tau_{dr} - \tau_{dl} = (F_{xfr} - F_{xfl}) r_\sigma \\ \tau_{dl} = F_{xfl} \cdot r_\sigma \\ \tau_{dr} = F_{xfr} \cdot r_\sigma \end{cases} , \tag{6}$$

where, J_e is the equivalent inertia moment of the steering system, b_e is the equivalent steering damping, ΔM is the difference between the moments of the two front wheels around their kingpins, $\tau_{\alpha l}$ and $\tau_{\alpha r}$ are the aligning moments of the left and right front wheels, τ_α is the total aligning moment of the front wheels, τ_f is the friction moment of the steering system, l is the half width of the tire grounding, r_σ is the scrub radius.

Because the dry friction torque of vehicle steering system, τ_f, is small and difficult to measure, its influence can be ignored. At the same time, because the value of $\ddot{\delta}_f$ is small, it can also be ignored. Due to the longitudinal force of the front wheel, $F_{xfj} = T_{fj}/R_c$, $(j = l, r)$, where R_c is
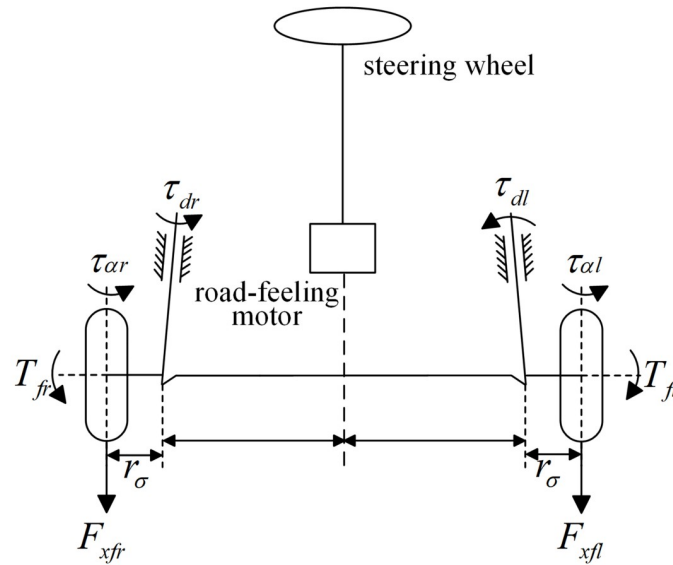
Fig 2. Front wheel differential steering system.

https://doi.org/10.1371/journal.pone.0285485.g002

the wheel radius, we can get:

$$\Delta M = (T_{fr} - T_{fl})\frac{r_\sigma}{R_c} = \frac{r_\sigma}{R_c}\Delta T, \tag{7}$$

where, ΔT is the differential driving torque between the left and right front wheels.

Substituting Eq (7) into Eq (6), then Eq (6) can be rewritten as:

$$\dot{\delta}_f = \frac{l^2 k_f}{3b_e}\delta_f - \frac{l^2 k_f}{3b_e v_x}v_y - \frac{l^2 k_f l_f}{3b_e v_x}\omega + \frac{r_\sigma}{b_e R_c}\Delta T. \tag{8}$$

Reference model

In this paper the typical two degree of freedom linear vehicle model is selected as the reference model to provide the ideal lateral velocity v_{yd}, and yaw rate ω_d under the premise of given front wheel steering angle δ_{fd}, and longitudinal velocity v_{xd}.

Set the state space variable as $x_d(t) = [\beta_d, \omega_d]$, and the system input as the front wheel steering angle δ_{fd}, that is, $u_d(t) = [\delta_{fd}]$, the corresponding state equation of the reference model is:

$$\begin{cases} \dot{x}_d = A_d x_d + B_d u_d \\ y_d = C_d x_d + D_d u_d \end{cases}, \tag{9}$$

$$A_d = \begin{pmatrix} \dfrac{(k_f + k_r)}{mv_{xd}} & \dfrac{(l_f k_f - l_r k_r)}{mv_{xd}^2} - 1 \\ \dfrac{(l_f k_f - l_r k_r)}{I_z} & \dfrac{(l_f^2 k_f + l_r^2 k_r)}{I_z v_{xd}} \end{pmatrix}, B_d = \begin{pmatrix} -\dfrac{k_f}{mv_{xd}} \\ -\dfrac{l_f k_f}{I_z} \end{pmatrix}, C_d = \begin{pmatrix} 1 & 0 \\ 0 & 1 \end{pmatrix}, D_d = \begin{pmatrix} 0 \\ 0 \end{pmatrix}.$$

According to the relationship between the sideslip angle and the lateral velocity, the ideal lateral velocity can be obtained as:

$$v_{yd} = v_{xd} \cdot \tan \beta_d. \tag{10}$$

Design of hierarchical control system

For the 4IWM EV with the differential steering, this paper designs a hierarchical control system as shown in Fig 3.

It can be seen from Fig 3 that the reference model outputs the ideal longitudinal velocity v_{xd}, the lateral velocity v_{yd} and the yaw rate ω_d under the given front wheel steering angle δ_{fd}. The upper controller calculates the expected longitudinal resultant force F_{xd}, lateral resultant force F_{yd} and resultant torque M_d required by the FWDSV model to track the reference model based on the actual longitudinal velocity v_x, lateral velocity v_y and yaw rate ω output from the FWDSV model. According to the objective function and constraint condition, the middle controller distributes the resultant forces and torque, F_{xd}, F_{yd} and M_d, into the longitudinal and lateral forces of the four wheels, i.e., $F_{yij}(i = f, r, j = l, r)$, $F''_{xfj}(j = l, r)$, $F_{xrj}(j = l, r)$, by the optimization solution.

The lower controller converts the lateral forces of four wheels $F_{yij}(i = f, r, j = l, r)$ into the front wheel steering angle δ_f and the tire sideslip angles of four wheels $\alpha_{ij}(i = f, r, j = l, r)$ through the tire inverse model. Then the front wheel steering angle δ_f is input to the FWDSS model to obtain the differential driving torque between the left and right front wheels ΔT, which is finally transformed to the longitudinal forces of the rear wheels $F_{xfj}(j = l, r)$. Finally, the longitudinal forces of the four wheels $F_{xij}(i = f, r, j = l, r)$ and the sideslip angles of four wheels $\alpha_{ij}(i = f, r, j = l, r)$ are also provided to the FWDSV model. In this way, the control system forms a closed loop.

Design of upper controller

Sliding mode variable structure control is a control method with strong robustness, which has the advantages of fast response and insensitive to the external changes and disturbances. The control of exponential reaching law can also effectively reduce the system jitter [29]. Therefore, it is used to design of the upper controller.
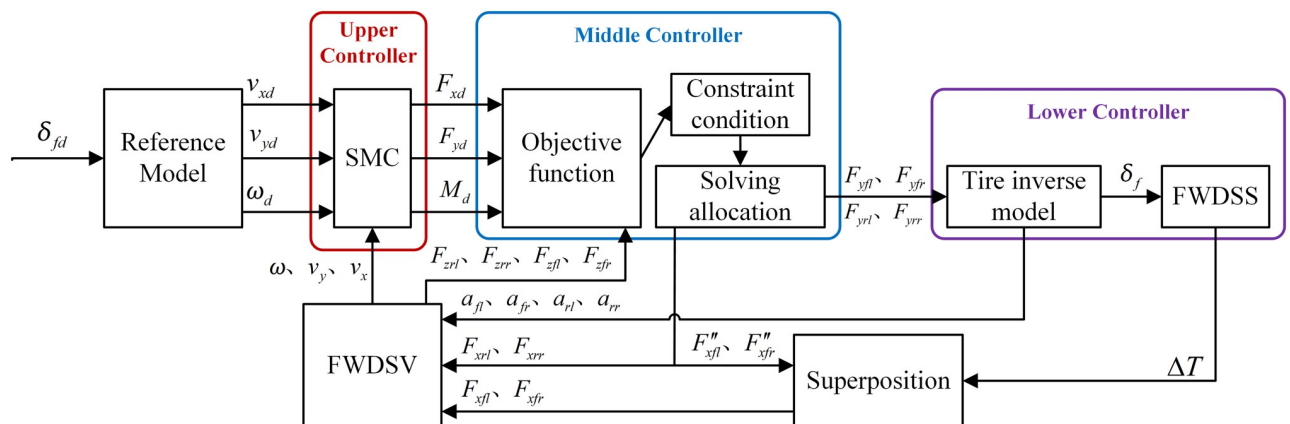

Fig 3. Hierarchical control system.

https://doi.org/10.1371/journal.pone.0285485.g003

According to the FWDSV model and the reference model established above, the tracking errors of the actual and ideal longitudinal velocities, lateral velocities and yaw rates are set as e_1, e_2, e_3, respectively.

$$\begin{cases} e_1 = v_x - v_{xd} \\ e_2 = v_y - v_{yd} \\ e_3 = \omega - \omega_d \end{cases}. \tag{11}$$

Different sliding surfaces are selected for the control of the longitudinal velocity, the lateral velocity and the yaw rate.

$$\begin{cases} s_1 = c_1 e_1 \\ s_2 = c_2 e_2 \\ s_3 = c_3 e_3 \end{cases}, \tag{12}$$

where, c_1, c_2, c_3 are the controller parameters that must meet the Hurwitz condition, and their values are greater than zero.

The exponential approach law is adopted to reduce the system chattering. The expression is as follows:

$$\begin{cases} \dot{s}_1 = -\varepsilon_1 \, \mathrm{sgn}\, s_1 - k_1 s_1 \\ \dot{s}_2 = -\varepsilon_2 \, \mathrm{sgn}\, s_2 - k_2 s_2 \\ \dot{s}_3 = -\varepsilon_3 \, \mathrm{sgn}\, s_3 - k_3 s_3 \end{cases}, \tag{13}$$

where, ε_1, ε_2, ε_3, k_1, k_2 and k_3 are the controller parameters, and their values are greater than zero.

In the process of sliding mode switching, by increasing k and decreasing ε at the same time, the system will be less affected and the transition will be more stable. From the accessibility of a sliding mode controller, $s = \dot{s} = 0$ must be satisfied, then

$$\begin{cases} \dot{v}_x = \dfrac{-\varepsilon_1 \, \mathrm{sgn}\, s_1 - k_1 s_1}{c_1} + \dot{v}_{xd} \\ \dot{v}_y = \dfrac{-\varepsilon_2 \, \mathrm{sgn}\, s_2 - k_2 s_2}{c_2} + \dot{v}_{yd} \\ \dot{\omega} = \dfrac{-\varepsilon_3 \, \mathrm{sgn}\, s_3 - k_3 s_3}{c_3} + \dot{\omega}_d \end{cases}. \tag{14}$$

In order to reduce the chattering of system, the sgn s in Eq (13) is replaced by a saturation function $sat(s_n/\Delta_n)$, where $n = 1, 2, 3$. And

$$sat(s_n/\Delta_n) = \begin{cases} s_n/\Delta_n & |s_n/\Delta_n| \leq 1 \\ \mathrm{sgn}(s_n/\Delta_n) & |s_n/\Delta_n| > 1 \end{cases}, \tag{15}$$

where, Δ_n is the boundary layer. The larger its value is, the less chattering will be. However, at the same time the approaching speed will slow down.

By combining Eqs (1) and (14), the output of the sliding mode controller can be solved, that is, the required resultant forces and torque.

$$\begin{cases} F_{xd} = m\left[\dfrac{-\varepsilon_1 sat(s_1/\Delta_1) - k_1 s_1}{c_1} + \dot{v}_{xd} - v_y\omega\right] \\ F_{yd} = m\left[\dfrac{-\varepsilon_2 sat(s_2/\Delta_2) - k_2 s_2}{c_2} + \dot{v}_{yd} + v_x\omega\right] \\ M_d = I_z\left[\dfrac{-\varepsilon_3 sat(s_3/\Delta_3) - k_3 s_3}{c_3} + \dot{\omega}_d\right] \end{cases}. \tag{16}$$

Design of middle controller

In this section, the expected resultant forces and torque obtained by the upper controller should be optimally decomposed into the longitudinal and transverse forces of four wheels according to the objective function. Therefore, the objective function, constraint conditions and optimization solution will be researched in the following.

Objective function. Considering that the tire load ratio represents the stability margin of the tire, and the lower the tire load ratio, the greater the stability margin. Therefore, in this paper the minimum tire load ratio is selected as the optimization objective. The so-called tire load ratio refers to the ratio of the adhesion force between the single wheel and the ground to the maximum adhesion force under the current road conditions. And the objective function can be expressed as [30]:

$$\min J = \sum_{i=l}^{r}\sum_{i=f}^{r}\frac{F_{xij}^2 + F_{yij}^2}{\mu^2 F_{zij}^2}, \tag{17}$$

where, μ is the adhesion coefficient of the road where the tires are located.

The value range of tire load ratio is [0,1]. The smaller the tire load ratio is, the more force the tire can output and the greater the stability margin is. In other words, the closer the tire load ratio is to 1, the worse the controllability of the vehicle is. When the tire load ratio equals to 1, it indicates that the tire has reached the limit of its adhesion capacity. If the vehicle is disturbed at this time, it will lose stability because the tire has no residual force to respond to this disturbance.

Constraint conditions. During driving, the 4WIM EV will be affected and limited by the tire friction circle, the maximum driving force of the in-wheel-motor, the resultant forces and resultant torque of the vehicle, therefore it is necessary to define some constraints on the solution of the objective function.

Constraint of tire friction circle. Generally, the tire adhesion limit of each wheel shall be regarded as a constraint condition, which can be described by the tire friction circle. That is to say, the following expression shall be met between the tire longitudinal and lateral forces, and vertical load.

$$F_{xij}^{\;2} + F_{yij}^{\;2} \le \left(\mu F_{zij}\right)^2, (i = f, r, j = l, r). \tag{18}$$

In this paper, the nonlinear tire friction circle constraint is simplified to a linear polygon constraint. In order to ensure that the longitudinal and lateral forces of each wheel do not exceed the friction circle, a safe friction circle is set up, that is, multiplying the friction circle in Eq (18) by a safety factor of 0.9, and then circumscribing an octagon on the safe friction circle to obtain the required linear constraint, as shown in Fig 4.
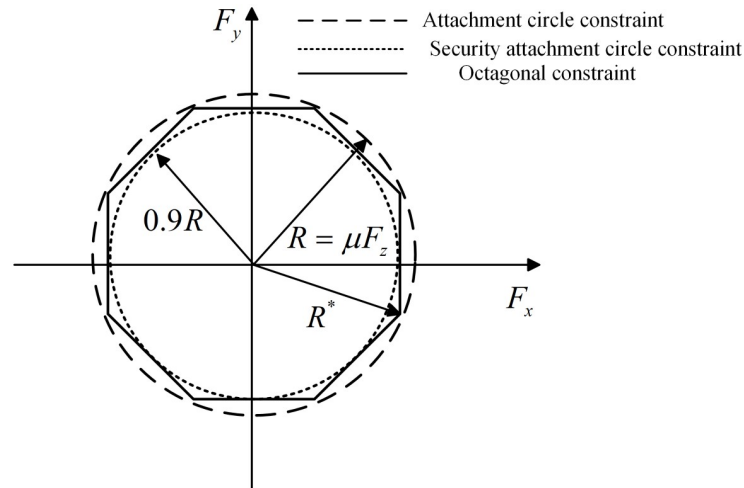
Fig 4. Linear simplified model of tire friction circle.

The radius of the attached circle in Fig 4 is μF_z, and the circumscribed circle radius of the octagon is calculated as follows:

$$R^* = 0.9R \cdot \sec 22.5^\circ \approx 0.97R < R. \tag{19}$$

Because the radius of the octagonal circumscribed circle is smaller than that of the tire friction circle, each tire force can be limited in the tire friction circle, and its specific linear constraint equation can be described as follows:

$$\begin{cases} -0.9\mu F_{zij} \leq F_{xij} \leq 0.9\mu F_{zij} \\ -0.9\mu F_{zij} \leq F_{yij} \leq 0.9\mu F_{zij} \\ -\sqrt{2} \cdot 0.9\mu F_{zij} \leq F_{xij} + F_{yij} \leq \sqrt{2} \cdot 0.9\mu F_{zij} \\ -\sqrt{2} \cdot 0.9\mu F_{zij} \leq -F_{xij} + F_{yij} \leq \sqrt{2} \cdot 0.9\mu F_{zij} \end{cases} . \tag{20}$$

Constraint of in-wheel-motor maximum driving force. In this paper the driving force of each wheel is independently controlled by the in-wheel-motor, whose driving torque is limited. Therefore, the longitudinal forces provided by the four tires are limited as follows:

$$-T_{\max}/R_c \leq F_{xij} \leq T_{\max}/R_c, (i = f, r, j = l, r). \tag{21}$$

where, $T_{\max}$ is the maximum torque of the motor, and the value is $600 \, N \cdot m$.

Constraint of resultant force and torque. The expected resultant forces and torque output by the upper controller must be provided by each wheel, so that the constraint of the resultant forces and torque can be obtained as follows:

$$\begin{cases} F_{xd} = F_{xfl} + F_{xfr} + F_{xrl} + F_{xrr} \\ F_{yd} = F_{yfl} + F_{yfr} + F_{yrl} + F_{yrr} \\ M_d = l_f\left(F_{yfl} + F_{yfr}\right) - l_r\left(F_{yrl} + F_{yrr}\right) + l_s\left(F_{xfr} - F_{xfl}\right) \end{cases} . \tag{22}$$

Optimization solution. Optimization problem is a typical nonlinear control problem. At present, the commonly used optimization algorithms include quadratic programming optimization algorithm, genetic algorithm, particle swarm optimization algorithm [31], etc. Considering that quadratic programming optimization algorithm can be used to solve complex problems or problems with equality and inequality constraints [20], and has high dynamic distribution accuracy and good real-time performance, it is selected to solve the objective function in this paper.

The so-called quadratic programming problem is an optimization problem in which the objective function is a quadratic function and the constraint function is a linear function. Let $x^T = (F_{xfl}, F_{yfl}, F_{xfr}, F_{yfr}, F_{xrl}, F_{yrl}, F_{xrr}, F_{yrr})$, then the objective function (17) can be rewritten into the standard form of quadratic programming, inequalities (18) and (20) can be written as $Ax \leq b$, Eq (22) can be written as $A_{eq}x = b_{eq}$, and inequality (21) describing the value range of state variables can be rewritten into $lb \leq x \leq ub$, namely:

$$\min_x f(x) = \frac{1}{2}x^T H x + f^T x, \tag{23}$$

$$\text{s.t.} \begin{cases} Ax \leq b \\ A_{eq}x = b_{eq} \\ lb \leq x \leq ub \end{cases}, \tag{24}$$

where,

$$H = \frac{2}{\mu^2} diag\left(\frac{1}{F_{zfl}{}^2}, \frac{1}{F_{zfl}{}^2}, \frac{1}{F_{zfr}{}^2}, \frac{1}{F_{zfr}{}^2}, \frac{1}{F_{zrl}{}^2}, \frac{1}{F_{zrl}{}^2}, \frac{1}{F_{zrr}{}^2}, \frac{1}{F_{zrr}{}^2}\right),$$

$$f = [0; 0; 0; 0; 0; 0; 0; 0],$$

$$A = \begin{bmatrix}
1\,0\,0\,0\,0\,0\,0\,0; & -1\,0\,0\,0\,0\,0\,0\,0; & 0\,0\,1\,0\,0\,0\,0\,0; \\
0\,0\,-1\,0\,0\,0\,0\,0; & 0\,0\,0\,0\,1\,0\,0\,0; & 0\,0\,0\,0\,-1\,0\,0\,0; \\
0\,0\,0\,0\,0\,0\,1\,0; & 0\,0\,0\,0\,0\,0\,-1\,0; & 0\,1\,0\,0\,0\,0\,0\,0; \\
0\,-1\,0\,0\,0\,0\,0\,0; & 0\,0\,0\,1\,0\,0\,0\,0; & 0\,0\,0\,-1\,0\,0\,0\,0; \\
0\,0\,0\,0\,0\,1\,0\,0; & 0\,0\,0\,0\,0\,-1\,0\,0; & 0\,0\,0\,0\,0\,0\,0\,1; \\
0\,0\,0\,0\,0\,0\,0\,-1; & 1\,1\,0\,0\,0\,0\,0\,0; & -1\,-1\,0\,0\,0\,0\,0\,0; \\
0\,0\,1\,1\,0\,0\,0\,0; & 0\,0\,-1\,-1\,0\,0\,0\,0; & 0\,0\,0\,0\,1\,1\,0\,0; \\
0\,0\,0\,0\,-1\,-1\,0\,0; & 0\,0\,0\,0\,0\,0\,1\,1; & 0\,0\,0\,0\,0\,0\,-1\,-1; \\
-1\,1\,0\,0\,0\,0\,0\,0; & 1\,-1\,0\,0\,0\,0\,0\,0; & 0\,0\,-1\,1\,0\,0\,0\,0; \\
0\,0\,1\,-1\,0\,0\,0\,0; & 0\,0\,0\,0\,-1\,1\,0\,0; & 0\,0\,0\,0\,1\,-1\,0\,0; \\
0\,0\,0\,0\,0\,0\,-1\,1; & 0\,0\,0\,0\,0\,0\,1\,-1
\end{bmatrix},$$

$$b = \begin{bmatrix}
0.9\mu F_{zfl}; 0.9\mu F_{zfl}; 0.9\mu F_{zfr}; 0.9\mu F_{zfr}; 0.9\mu F_{zrl}; 0.9\mu F_{zrl}; \\
0.9\mu F_{zrr}; 0.9\mu F_{zrr}; 0.9\mu F_{zfl}; 0.9\mu F_{zfl}; 0.9\mu F_{zfr}; 0.9\mu F_{zfr}; \\
0.9\mu F_{zrl}; 0.9\mu F_{zrl}; 0.9\mu F_{zrr}; 0.9\mu F_{zrr}; 1.3\mu F_{zfl}; 1.3\mu F_{zfl}; \\
1.3\mu F_{zfr}; 1.3\mu F_{zfr}; 1.3\mu F_{zrl}; 1.3\mu F_{zrl}; 1.3\mu F_{zrr}; 1.3\mu F_{zrr}; \\
1.3\mu F_{zfl}; 1.3\mu F_{zfl}; 1.3\mu F_{zfr}; 1.3\mu F_{zfr}; 1.3\mu F_{zrl}; 1.3\mu F_{zrl}; \\
1.3\mu F_{zrr}; 1.3\mu F_{zrr}
\end{bmatrix},$$

$$A_{eq} = \begin{bmatrix} 1 & 0 & 1 & 0 & 1 & 0 & 1 & 0 \\ 0 & 1 & 0 & 1 & 0 & 1 & 0 & 1 \\ -l_s & l_f & l_s & l_f & 0 & -l_r & 0 & -l_r \end{bmatrix},$$

$$b_{eq} = \left[F_{xd}; F_{yd}; M_d \right],$$

$$l_b = \left[-\frac{T_{max}}{R_c}; -\frac{T_{max}}{R_c}; -\frac{T_{max}}{R_c}; -\frac{T_{max}}{R_c} \right],$$

$$u_b = \left[\frac{T_{max}}{R_c}; \frac{T_{max}}{R_c}; \frac{T_{max}}{R_c}; \frac{T_{max}}{R_c} \right].$$

If H is a positive semidefinite matrix, then $f(x)$ is a convex function. The corresponding quadratic programming is a convex quadratic programming problem. If there is a local optimal solution at this point, then this local optimal solution is the global optimal solution. But this global minimum may not be unique. If H is a positive definite matrix, then the problem has a unique global minimum. From the expression of H, it is not difficult to draw a conclusion that H in this paper is a positive definite matrix. Compiling the s-function in MATLAB/Simulink for Eqs (23) and (24), calling the function quadprog ($H,f,A,b,Aeq,beq,lb,ub,x_0$, options) provided by Matlab to solve the optimization problem, and the longitudinal and lateral forces required by each wheel can be calculated.

Design of lower controller

The purpose of the lower controller is to convert the lateral force of each wheel obtained by the middle controller into the tire sideslip angles of four wheels and the front wheel steering angle of the vehicle. And the latter will continue to be converted into the longitudinal forces of the front wheels by the tire inverse model. Then the two longitudinal forces of the front wheels are superimposed by the superposition scheme. That is to say, the longitudinal and lateral forces obtained by the middle controller are transformed to the longitudinal force and tire sideslip angle of each wheel required by the front wheel differential steering vehicle dynamics equation shown in Eq (4).

Tire inverse model. The control of tire longitudinal force can be directly realized through the control of in-wheel-motor driving or braking torque, but the control of tire lateral force cannot be directly realized. Therefore, it is necessary to use the tire inverse model to convert the tire lateral force into tire sideslip angle and the front wheel steering angle. There are two main methods to study the tire inverse model: look-up table method and analytical method. The former is to obtain the relationship table between the tire input variables and the tire force under various typical working conditions through experiments, and then find out the value of tire sideslip angle under the known conditions of tire longitudinal force, lateral force and road adhesion coefficient. Compared with the former, the tire inverse model based on the latter needs less data, which is more suitable for practical use.

The tire inverse mode adopted in this paper can be expressed as:

$$F_{yij} = -k_i G_{xij} \frac{\mu}{C_{ij}} \tan^{-1}\left(\frac{C_{ij}}{\mu}\alpha_{ij}\right), (i = f, r, j = l, r), \tag{25}$$

where, $G_{xij} = \sqrt{1 - \left(\frac{F_{xij}}{\mu F_{zij}}\right)^2}$, $C_{ij} = k_i \frac{\pi}{p} \frac{1}{F_{zij}}$, $p = 2.9$.

From Eq (25), the sideslip angle of each wheel for feedback to Eq (4) can be derived:

$$\alpha_{ij} = -\frac{\mu}{C_{ij}} \tan\left(\frac{C_{ij}}{\mu} \frac{1}{k_i G_{xij}} F_{yij}\right), (i = f, r, j = l, r). \tag{26}$$

The steering angles of the left and right front wheels can be expressed as:

$$\delta_{fj} = \tan^{-1}\left(\frac{v_y + \omega l_f}{v_x - \omega l_s}\right) - \alpha_{fj}, (j = l, r), \tag{27}$$

where, $\delta_{fj}(j = l, r)$ is the steering angle of the left/right front wheel.

Superposition scheme of longitudinal force. Let $\delta_f = (\delta_{fl} + \delta_{fr})/2$, and substitute it into Eq (8), the required front wheel differential driving torque ΔT can be obtained. According to this, the driving forces distributed to the left and right front wheels, F'_{xfl} and F'_{xfr}, are as follows:

$$\begin{cases} F'_{xfl} = -\dfrac{\Delta T}{2R_c} \\ F'_{xfr} = \dfrac{\Delta T}{2R_c} \end{cases}. \tag{28}$$

Let the longitudinal forces of the left and right front wheels obtained through optimization to be F''_{xfl} and F''_{xfr}, then the actual longitudinal forces of the left and right front wheels are as follows:

$$\begin{cases} F_{xfl} = F'_{xfl} + F''_{xfl} \\ F_{xfr} = F'_{xrl} + F''_{xfr} \end{cases}. \tag{29}$$

Simulation results

In order to verify the effectiveness of the proposed controller, the double lane change maneuver is selected to conduct the comparative simulation test on the reference model, the FWDSV with hierarchical controller, and the FWDSV with SMC controller which does not consider the tire friction circle (see [27] for details). The vehicle parameters used in the simulation are shown in Table 1. When the road adhesion coefficient is 0.8, $k_f = 95202 * 2N/rad$, $k_r = 63947 * 2N/rad$. When the road adhesion coefficient is 0.2, $k_f = 68000 * 2N/rad$, $k_r = 59000 * 2N/rad$.

High adhesion coefficient road

Under this working condition, the road adhesion coefficient is set to 0.8, the longitudinal speeds of the reference model and the FWDSV with SMC controller are set to 80km/h, and the steering wheel angle input of the reference model is shown in Fig 5A. The front wheel steering angles, yaw rates, sideslip angles and driving trajectory curves of the three models are shown in Fig 5B–5E.

Table 1. Vehicle simulation parameters.

Parameters	Values
b_e	$100N$
g	$10\ m/s^2$
h	$054m$
I_z	$1343kg \cdot m^2$
l	$0.0368m$
l_f	$1.04m$
l_r	$1.56m$
l_s	$0.74m$
m	$1240kg$
r	$0.0754m$
R_c	$0.298m$

It can be seen from Fig 5B–5E that all of the front-wheel steering angles, yaw rates, sideslip angles and driving trajectories of the FWDSVs with hierarchical controller and with SMC controller can track those of the reference model very well. And their extreme values are shown in Table 2.

From Table 2 we can see that the extreme values of the front-wheel steering angle, the yaw rate and the sideslip angle of the FWDSV with the hierarchical controller are closer to those of the reference model than those of the FWDSV with SMC controller. However, compared to FWDSV with SMC controllers, the extreme value of the lateral displacement of the FWDSV with the hierarchical controller is slightly greater than the lateral displacement of the reference model, it is also fully acceptable because of the 4m road width.

The longitudinal speeds of the reference model and the FWDSV with hierarchical controller are shown in Fig 5F, from which the conclusion can be drawn that the longitudinal speed of the FWDSV with hierarchical controller can still be well maintained at 80km/h even when the vehicle starts to turn. The tire load ratio curves of the FWDSVs with hierarchical controller and with SMC controller are shown in Fig 5G and 5H, respectively.

It can be seen from Fig 5H that the tire load ratios of four wheels of the FWDSV with SMC controller are basically evenly distributed. However, for the FWDSV with hierarchical controller the load ratios of rear wheels are significantly greater than those of front wheels, and the tire load ratios of the left and right wheels are also obviously different, as shown in Fig 5G. The reason why the rear wheel load ratio is greater than the front wheel is that the rear wheels are mainly used for driving, and the longitudinal forces on the rear wheels have to increase to keep the constant velocity during the steering. And the reason why the left and right wheel load ratios are not equal is that the load is redistributed on the left and right wheels when the vehicle is turning.

Low adhesion coefficient road

Under this working condition, the vehicle speed is 54km/h, the road adhesion coefficient is 0.2, the steering wheel angle input of the reference model is shown in Fig 6A. The simulation results of the three models are shown in Fig 6B–6H.

It can be seen from Fig 6B–6E that all of the front-wheel steering angle, yaw rate, sideslip angle and driving trajectory of the FWDSVs with SMC controller can track those of the reference model very well, but those of the FWDSV with hierarchical controller are significantly different from those of the reference model. And their extreme values are shown in Table 3.
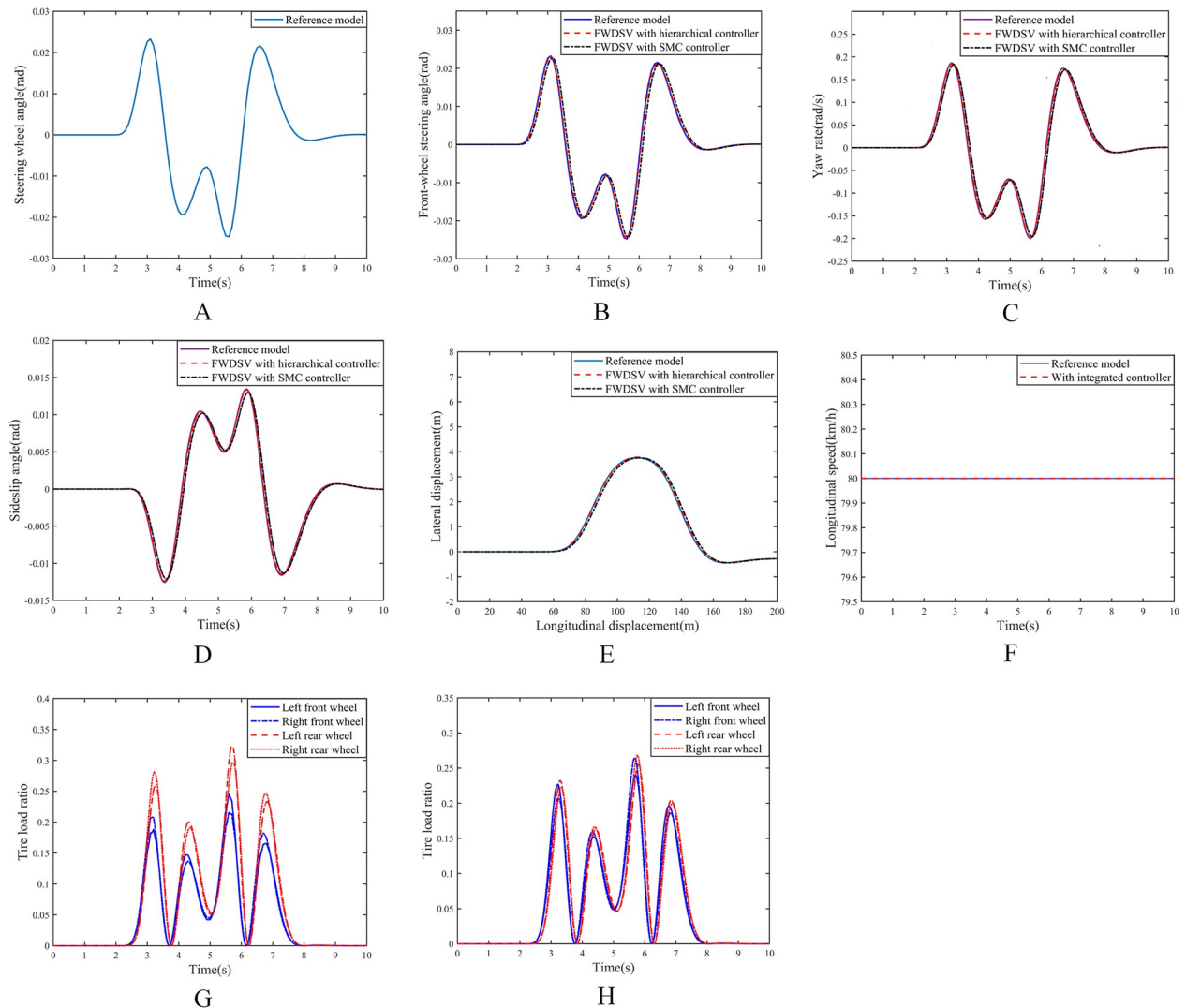
Fig 5. Simulation results on high adhesion coefficient road. (A) Input of steering wheel angle. (B) Curve of front wheel steering angles. (C) Curve of yaw rates. (D) Curve of sideslip angles. (E) Curve of vehicle trajectories. (F) Curve of longitudinal speeds. (G) Tire load ratio of FWDSV with hierarchical controller. (H) Tire load ratio of FWDSV with SMC controller.

From Table 3 we can see that the extreme values of the front-wheel steering angle, the yaw rate, the sideslip angle and the lateral displacement of the FWDSV with SMC controller are closer to those of the reference model than those of the FWDSV with hierarchical controller. However, compared to FWDSV with SMC controllers, the extreme value of the lateral

Table 2. Extreme values of response curves for three models on high adhesion coefficient road.

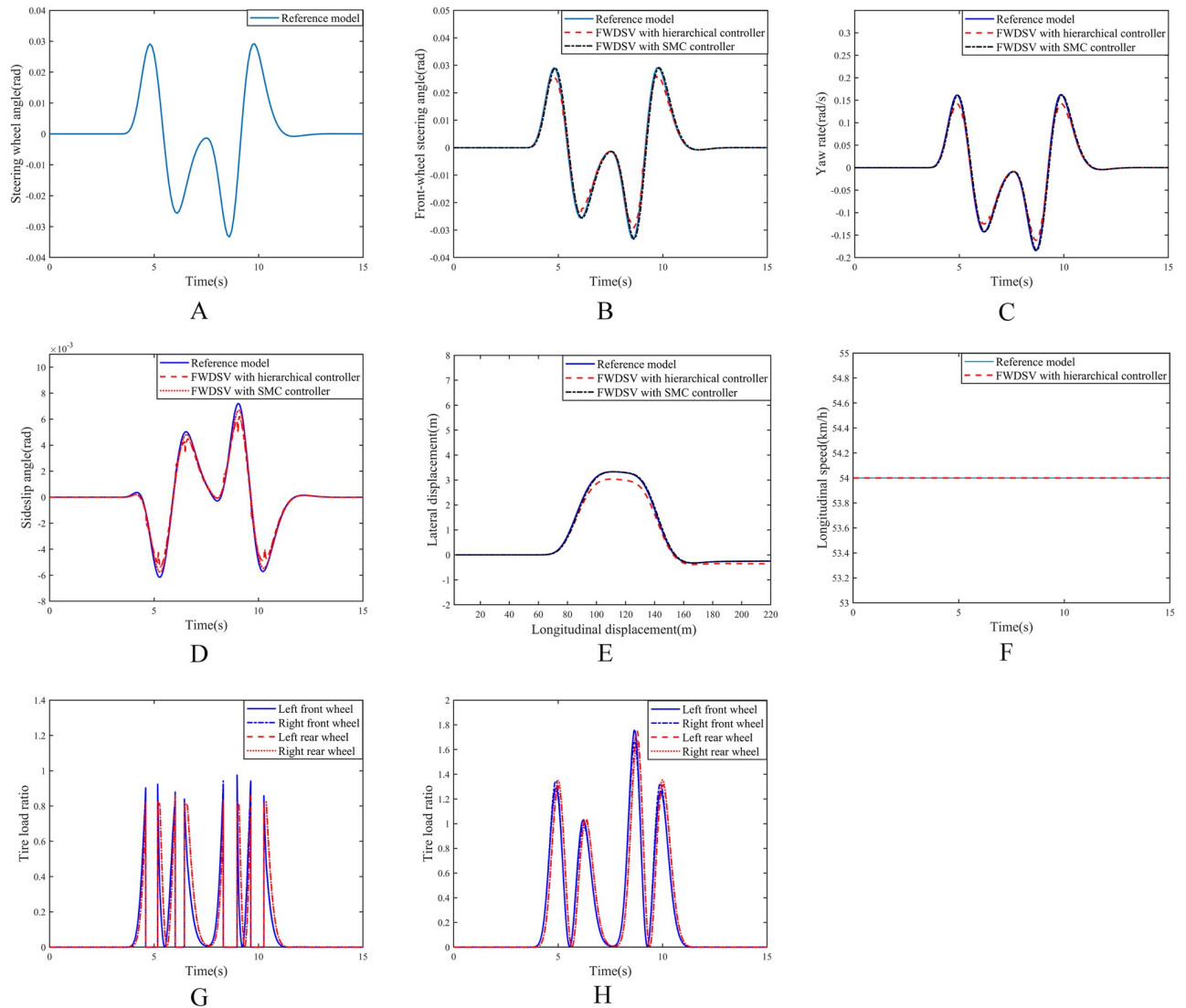|	Front-wheel steering angle (maximum)	Yaw rate (maximum)	Sideslip angle (minimum)	Lateral displacement (maximum)
Reference model	0.0232rad	0.1866rad/s	-0.0125rad	3.7581m
FWDSV with hierarchical controller	0.0231rad	0.1845rad/s	-0.0124rad	3.7793m
FWDSV with SMC controller	0.0228rad	0.1833rad/s	-0.0121rad	3.7547m

Fig 6. Simulation results on low adhesion coefficient road. (A) Input of steering wheel angle. (B) Curve of front wheel steering angles. (C) Curve of yaw rates. (D) Curve of sideslip angles. (E) Curve of vehicle trajectories. (F) Curve of longitudinal speeds. (G) Tire load ratio of FWDSV with hierarchical controller. (H) Tire load ratio of FWDSV with SMC controller.

Table 3. Extreme values of response curves for three models on low adhesion coefficient road.

	Front-wheel steering angle (maximum)	Yaw rate (maximum)	Sideslip angle (minimum)	Lateral displacement (maximum)
Reference model	0.0291rad	0.1614rad/s	-0.0062rad	3.3302m
FWDSVs with hierarchical controller	0.0254rad	0.1414rad/s	-0.0054rad	3.0353m
FWDSVs with SMC controller	0.0289rad	0.1599rad/s	-0.0057rad	3.3283m

displacement of the FWDSV with hierarchical controller is slightly greater than the lateral displacement of the reference model, it is also fully acceptable because the road width is 4m.

The longitudinal speeds of the reference model and the FWDSV with hierarchical controller are shown in Fig 6F. It can be drawn that even on the low adhesion coefficient road the longitudinal speed of the FWDSV with hierarchical controller can still be stable at 54km/h. Fig 6G and 6H respectively show the tire load ratios of the FWDSVs with hierarchical controller and with SMC controller. It can be seen that on the low adhesion coefficient road, both of the tire load ratios are increased. However, all of the tire load ratios of the FWDSV with SMC controller exceed 1, and the maximum value even reaches 1.76 which is completely impossible in the actual situation.

Discussion

From the analysis of Fig 5, it can be seen that on the road with high adhesion coefficient, both of the FWDSVs with hierarchical controller and with SMC controller can well track the front wheel angle, yaw rate, sideslip angle, driving trajectory and longitudinal speed of the reference model. The reason is that the road adhesion coefficient is high and the tire force is not saturated. However, the tire load ratios of the four wheels of the SMC controlled FWDSV are almost equal, and the reason why the load ratios of the rear wheels of the hierarchical controlled FWDSV are higher than those of the front wheels is that the speed of the SMC controlled FWDSV is assumed to be constant, while the hierarchical controlled FWDSV needs to realize the constant speed of the FWDSV through the driving forces of the rear wheels. In addition, the reason why the load ratios of the left and right wheels of the hierarchical controlled FWDSV are not equal is that the load is redistributed on the left and right wheels during the driving process of the vehicle. And it can be drawn that the tire load ratios of the FWDSV with hierarchical controller is more reasonably distributed according to the change of wheel vertical load, although both of the tire load ratios are not high.

Remark 3. Performance in all aspects of the FWDSVs with hierarchical controller and with SMC controller can well track those of the reference model on the road with high coefficient of adhesion. The reason is that the adhesion relationship between the tire and the ground can be maintained stably on high adhesion coefficient road. Although the tire load ratios of the FWDSV with hierarchical controller are different from those of the FWDSV with SMC controller, the tire load ratios of the FWDSV with SMC controller do not exceed the limit, therefore both of the vehicles can track the reference model very well.

From the analysis of Fig 6, it can be seen that the FWDSV with SMC controller can well track the front wheel angle, yaw rate, sideslip angle, driving trajectory and longitudinal speed of the reference model on the road with low coefficient of adhesion, while those of the FWDSV with hierarchical controller has some deviations from those of the reference model. This is because the FWDSV with SMC controller does not consider the tire friction circle, and the vehicle speed is assumed to be constant, and the corresponding steering is only achieved by the differential driving torque of the left and right wheels, however, the load ratio of all tires is greater than 1. This is completely inconsistent with the actual situation. Although the FWDSV with hierarchical controller has some deviations in some performance, it can ensure that all tire load ratios are less than 1 which means that this control is feasible for vehicles.

Remark 4. Performance in all aspects of the FWDSV with SMC controller can track those of the reference model well on low adhesion coefficient road, while those of the FWDSV with hierarchical controller have some deviations. This is because the tire friction circle is not considered for the FWDSV with SMC controller. That is to say, because the tire force saturation is not considered, each performance of the FWDSV model with SMC controller can track those

of the reference model, but all of the tire load ratios are greater than 1. However, the hierarchical controller takes into account the nonlinearity of the tire and the limitations of the friction circle. Therefore, although there is a little deviation in each performance, the tire load ratios are not greater than 1. It can be drawn that the hierarchical controller proposed in this paper is effective.

Conclusion

1. This paper focuses on how to use the over-actuation drive system to realize the differential steering for four-wheel-motor electric vehicles. The so-called differential steering refers to the steering of the vehicle through the differential driving torque between the left and right front wheels. It can not only be used as the backup system of the steering-by-wire system, but also as the single steering system of the vehicle which can make the vehicle structure simpler.

2. However, if the load of a front wheel on one side is sharply reduced due to the redistribution of the load when the vehicle is turning, the actual driving torque of the wheel will be affected which may lead to the failure of differential steering. Therefore, this paper considers the problem of tire friction circle, and designs a hierarchical control strategy to ensure that the differential steering is realized while the vehicle speed is constant.

3. Firstly, the dynamic models of the front wheel differential steering vehicle, the front wheel differential steering system and the reference vehicle are established. Then the upper controller, the middle controller and the lower controller are designed respectively.

4. Finally, simulation results show that compared with SMC controller, the FWDSV with hierarchical controller can guarantee the vehicle to track the reference model well on both of the high and low adhesion coefficient roads, and all of the tire load ratios are smaller than 1 which prove that the hierarchical controller proposed in this paper is effective.

Author Contributions

Data curation: Mingfei Yang.

Investigation: Jie Tian.

Methodology: Jie Tian.

Software: Mingfei Yang.

Validation: Jie Tian.

Writing – original draft: Mingfei Yang.

Writing – review & editing: Jie Tian.

References

1. Zhang H, Zhang X, Wang J. Robust gain-scheduling energy-to-peak control of vehicle lateral dynamics stabilisation. Vehicle System Dynamics. 2014; 52(3): 309–40. https://doi.org/10.1080/00423114.2013.879190

2. Kuslits M, Bestle D. Multiobjective performance optimisation of a new differential steering concept. Vehicle System Dynamics. 2022; 60(1): 73–95. https://doi.org/10.1080/00423114.2020.1804598

3. Zhang L, Wang Z, Ding X, Li S, Wang Z. Fault-Tolerant Control for Intelligent Electrified Vehicles Against Front Wheel Steering Angle Sensor Faults During Trajectory Tracking. IEEE Access. 2021; 9: 65174–86. https://doi.org/10.1109/ACCESS.2021.3075325

4. Wang Z, Ding X, Zhang L. Chassis Coordinated Control for Full X-By-Wire Four-Wheel-Independent-Drive Electric Vehicles. IEEE Transactions on Vehicular Technology. 2022; 1–17. https://doi.org/10.1109/TVT.2022.3222778

5. Cai H, Xu X. Lateral Stability Control of a Tractor-Semitrailer at High Speed. Machines. 2022; 10(8): 716. https://doi.org/10.3390/machines10080716

6. Liu J, Wang Z, Zhang L. Integrated Vehicle-Following Control for Four-Wheel-Independent-Drive Electric Vehicles Against Non-Ideal V2X Communication. IEEE Transactions on Vehicular Technology. 2022; 71(4): 3648–59. https://doi.org/10.1109/TVT.2022.3141732

7. Xu X, Zhang L, Jiang Y, Chen N. Active Control on Path Following and Lateral Stability for Truck–Trailer Combinations. Arabian Journal for Science and Engineering. 2019; 44(2): 1365–77. https://doi.org/10.1007/s13369-018-3527-1

8. Zheng C, Xu D, Cao J, Li W. Design of lightweight electric forestry monotail vehicle. Journal of Forestry Engineering. 2021; 6(05): 140–6. https://doi.org/10.13360/j.issn.2096-1359.202012007

9. Li D, Xu B, Tian J, Ma Z. Energy Management Strategy for Fuel Cell and Battery Hybrid Vehicle Based on Fuzzy Logic. Processes. 2020; 8(8): 882. https://doi.org/10.3390/pr8080882

10. Li Y, Li D, Ma Z, Zheng M, Lu Z. Thermodynamic Modeling and Performance Analysis of Vehicular High-Temperature Proton Exchange Membrane Fuel Cell System. Membranes. 2022; 12(1): 72. https://doi.org/10.3390/membranes12010072 PMID: 35054598

11. Li D, Li Y, Ma Z, Zheng M, Lu Z. Exergetic Performance Coefficient Analysis and Optimization of a High-Temperature Proton Exchange Membrane Fuel Cell. Membranes. 2022; 12(1): 70. https://doi.org/10.3390/membranes12010070 PMID: 35054596

12. Wang H, Zheng Y, Yu Y. Lithium-Ion Battery SOC Estimation Based on Adaptive Forgetting Factor Least Squares Online Identification and Unscented Kalman Filter. Mathematics. 2021; 9(15): 1733. https://doi.org/10.3390/math9151733

13. Zhou W, Zheng Y, Pan Z, Lu Q. Review on the Battery Model and SOC Estimation Method. Processes. 2021; 9(9): 1685. https://doi.org/10.3390/pr9091685

14. Wang J, Zhang J, Yu Y, Zhang Y, Zhu X, Yue H, et al. Synthesis of Si /C composites derived from directly-carbonized reed plants as high-performance anode for lithium ion batteries. Journal of Forestry Engineering. 2019; 4(05): 84–91. https://doi.org/10.13360/j.issn.2096-1359.2019.05.012

15. Cheng Z, Zhou H, Lu Z. A Novel 10-Parameter Motor Efficiency Model Based on I-SA and Its Comparative Application of Energy Utilization Efficiency in Different Driving Modes for Electric Tractor. Agriculture. 2022; 12(3): 362. https://doi.org/10.3390/agriculture12030362

16. Cheng Z, Lu Z. Research on Load Disturbance Based Variable Speed PID Control and a Novel Denoising Method Based Effect Evaluation of HST for Agricultural Machinery. Agriculture. 2021; 11(10): 960. https://doi.org/10.3390/agriculture11100960

17. Cheng Z, Lu Z. Two novel reconstruction methods of sparsity adaptive adjustment for road roughness compressive signal based on I-SA and GSM. Mechanical Syetems And Signal Processing. 2022; 171. https://doi.org/10.1016/j.ymssp.2022.108915

18. Sun S, Wan M, Wang H, Zhang Y, Xu Xiao M. Study of component high cycle bending fatigue based on a new critical distance approach. Engineering Failure Analysis. 2019; 102: 395–406. https://doi.org/10.1016/j.engfailanal.2019.04.050

19. Sun S, Liu W, Zhang X, Wan M. Crankshaft HCF Research Based on the Simulation of Electromagnetic Induction Quenching Approach and a New Fatigue Damage Model. Metals. 2022; 12(8): 1296. https://doi.org/10.3390/met12081296

20. Jing H, Wang R, Li C, Wang J. Differential steering-based electric vehicle lateral dynamics control with rollover consideration. Proceedings of the Institution of Mechanical Engineers, Part I: Journal of Systems and Control Engineering. 2019; 234(3): 338–48. https://doi.org/10.1177/0959651819855810

21. Chen T, Cai Y, Chen L, Xu X, Sun X. Trajectory tracking control of steer-by-wire autonomous ground vehicle considering the complete failure of vehicle steering motor. Simulation Modelling Practice and Theory. 2021; 109: 102235. https://doi.org/10.1016/j.simpat.2020.102235

22. Hu C, Wang R, Qin Y, editors. Adaptive Multivariable Super-Twisting Control for Lane Keeping of Autonomous Vehicles with Differential Steering. 2018 IEEE Intelligent Vehicles Symposium (IV); 2018 26–30 June 2018.

23. Hu C, Wang R, Yan F, Huang Y, Wang H, Wei C. Differential Steering Based Yaw Stabilization Using ISMC for Independently Actuated Electric Vehicles. IEEE Transactions on Intelligent Transportation Systems. 2018; 19(2): 627–38. https://doi.org/10.1109/TITS.2017.2750063

24. Kuslits M, Bestle D. Modelling and control of a new differential steering concept. Vehicle System Dynamics. 2019; 57(4): 520–42. https://doi.org/10.1080/00423114.2018.1473616

25. Khan MA, Aftab MF, Ahmed E, Youn I. Robust Differential Steering Control System for an Independent Four Wheel Drive Electric Vehicle. International Journal of Automotive Technology. 2019; 20(1): 87–97. https://doi.org/10.1007/s12239-019-0008-9

26. Tian J, Tong J, Luo S. Differential Steering Control of Four-Wheel Independent-Drive Electric Vehicles. Energies. 2018; 11(11): 2892. https://doi.org/10.3390/en11112892

27. Tian J, Ding J, Zhang C, Luo S. Four-Wheel Differential Steering Control of IWM Driven EVs. IEEE Access. 2020; 8: 152963–74. https://doi.org/10.1109/ACCESS.2020.3017759

28. Fahimi F. Full drive-by-wire dynamic control for four-wheel-steer all-wheel-drive vehicles. Vehicle System Dynamics. 2013; 51(3): 360–76. https://doi.org/10.1080/00423114.2012.743668

29. Zhang B, Zong C, Chen G, Huang Y, Xu T. A Novel Integrated Stability Control Based on Differential Braking and Active Steering for Four-axle Trucks. Chinese Journal of Mechanical Engineering. 2019; 32(1): 12. https://doi.org/10.1186/s10033-019-0323-0

30. Peng H, Wang W, Xiang C, Li L, Wang X. Torque Coordinated Control of Four In-Wheel Motor Independent-Drive Vehicles With Consideration of the Safety and Economy. IEEE Transactions on Vehicular Technology. 2019; 68(10): 9604–18. https://doi.org/10.1109/TVT.2019.2935617

31. Li H, Wang L, Wang F, Li Z. Research on multi-objective optimization of support parameters of high-speed railway tunnel. Journal of Forestry Engineering. 2021; 6(05): 169–75. https://doi.org/10.13360/j.issn.2096-1359.202012035